Spine

SPINE Volume 39, Number 13, pp 1018-1028
©2014, Lippincott Williams & Wilkins

BIOMECHANICS

How Healthy Discs Herniate

A Biomechanical and Microstructural Study Investigating the Combined Effects of Compression Rate and Flexion

Kelly R. Wade, PhD,* Peter A. Robertson, MD,† Ashvin Thambyah, PhD,* and Neil D. Broom, PhD*

Study Design. Microstructural investigation of compression-induced disruption of the flexed lumbar disc.

Objective. To provide a microstructural analysis of the mechanisms of annular wall failure in healthy discs subjected to flexion and an elevated rate of compression.

Summary of Background Data. At the level of the motion segment failure of the disc in compression has been extensively studied. However, at the microstructural level the exact mechanisms of disc failure are still poorly understood, especially in relation to loading posture and rate.

Methods. Seventy-two healthy mature ovine lumbar motion segments were compressed to failure in either a neutral posture or in high physiological flexion (10º) at a displacement rate of either 2 mm/min (low) or 40 mm/min (high). Testing at the high rate was terminated at stages ranging from initial wall tearing through to facet fracture so as to capture the evolution of failure up to full herniation. The damaged discs were then analyzed microstructurally.

Results. Approximately, 50% of the motion segments compressed in flexion at the high rate experienced annulus or annulus-endplate junction failure, the remainder failed *via* endplate fracture with no detectable wall damage. The average load to induce disc failure in flexion was 18% lower ($P < 0.05$) than that required to induce endplate fracture. Microstructural analysis indicated that wall rupture occurred first in the posterior mid-then-outer annulus.

Conclusion. Disc wall failure in healthy motion segments requires both flexion and an elevated rate of compression. Damage is initiated in the mid-then-outer annular fibers, this a likely consequence of the higher strain burden in these same fibers arising from endplate curvature. Given the similarity in geometry between ovine and human endplates, it is proposed that comparable mechanisms of damage initiation and herniation occur in human lumbar discs.

Key words: ovine lumbar motion segments, elevated rate of compression, flexion, microstructural analysis, annular disruption, mechanism of herniation.

Level of Evidence: N/A

Spine 2014;39:1018–1028

Lumbar disc herniation is the most common cause of sciatica and annular disruption may stimulate nerve endings in the outer annulus leading to low back pain.[1–3] The majority of biomechanical studies attempting to reproduce herniation have compressed motion segments in a fixed posture until failure occurs. Unflexed segments fail *via* endplate fracture or vertebral body compression,[4–9] while flexion increases the likelihood of annular failure[10–13] although the mechanisms of disc herniation are still poorly understood at the microstructural level.

Other studies have employed internal pressurization of motion segments with resected facet joints, combined with different postures.[14–17] Although these experiments provided some insight into modes of disc failure, the conditions used were somewhat removed from the *in vivo* state. This new study sought to provide a detailed microstructural analysis of the mechanisms of annular wall disruption in physiologically flexed healthy discs, after their compression at different loading rates.

MATERIALS AND METHODS

Lumbar spines from skeletally mature female ovine animals, 3 to 5 years in age, were stored for up to 6 months at −28°C, thawed before testing and extraneous soft tissues removed prior to dissection into L1–L2, L3–L4, and L5–L6 motion segments. We excluded spines with visible evidence of degeneration[18] based on a macroscopic inspection of transected discs adjacent to each prepared motion segment. The facets were preserved to maintain physiological motion. After rehydration in saline at 4°C the motion segments were mounted in stainless steel cups and fixed with dental plaster. Using a custom rig (Figure 1)[19] the segments were loaded in

From the *Department of Chemical and Materials Engineering, Experimental Tissue Mechanics Laboratory, University of Auckland, New Zealand; and; †Department of Orthopaedic Surgery, Auckland City Hospital, New Zealand.

Acknowledgment date: October 11, 2013. Revision date: January 20, 2014. Acceptance date: January 25, 2014.

The manuscript submitted does not contain information about medical device(s)/drug(s).

AO Foundation (project S-12-24B) grant funds were received in support of this work.

Relevant financial activities outside the submitted work: consultancy, grants, patents, royalties.

Address correspondence and reprint requests to Neil D. Broom, PhD, Department of Chemical and Materials Engineering, University of Auckland, Private Bag 92019, Auckland 1142, New Zealand; E-mail: nd.broom@auckland.ac.nz

DOI: 10.1097/BRS.0000000000000262

Copyright © 2014 Lippincott Williams & Wilkins. Unauthorized reproduction of this article is prohibited.

compression in either a neutral or flexed posture of 10°, this representing the physiological extreme of flexion in the ovine lumbar spine.[17] Ovine spines were used in this investigation because they have been shown to be similar to human spines in terms of anatomy,[20,21] biochemistry,[21] and biomechanics,[22] especially in the lumbar region. Despite the fact that sheep are quadrupeds, their spinal column is known to experience axial loading (as does the human spine) due to the muscle reaction forces acting upon it.[23]

Two different compression velocities were employed: low (2 mm/min) and high (40 mm/min), this high rate being sufficient to minimize creep and thus approximate traumatic physiological loading.[16,24] Video and sound recordings provided both a macroscopic visualization of disc response and audible evidence of rupture, which when combined with the load-displacement curves, enhanced our detection of the failure sequence. Failure load differences were analyzed for statistical significance using *t* tests and ANOVA in SPSS software (version 21; IBM Corp., Armonk, NY).

After testing to failure, the samples were fixed in formalin and decalcified in formic acid. They were then cut into quadrants, examined macroscopically, then cryosectioned into 30-μm–thick slices and microscopically analyzed for damage in their fully hydrated state. Failure modes were initially categorized into endplate fracture or annular damage, the latter then further classified according to both region (Figure 2) and severity of damage.

Seventy-two healthy motion segments from 25 ovine lumbar spines were tested as summarized in Table 1. Twelve were loaded only to a level sufficient to induce the 10° of flexion at 40 mm/min to verify that this degree of flexion alone was not injurious to the discs (these serving as reference motion segments); 17 were compressed to failure at 2 mm/min, 8 in neutral posture and 9 flexed 10°; 43 were compressed to failure at 40 mm/min, 19 in neutral posture, and 24 flexed 10°.

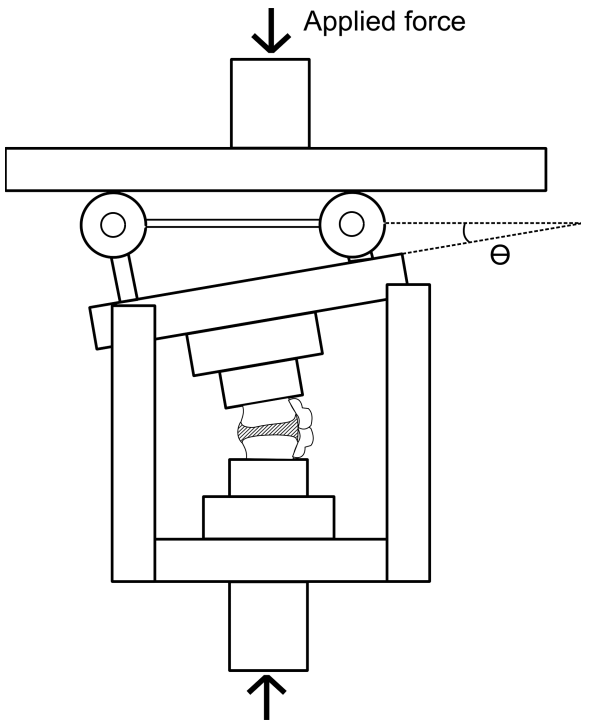

Figure 1. Rig used to compress motion segments with or without flexion (θ) as set by roller height difference. Vertical pillars constrain the upper plate to a single plane of motion thus eliminating torsion.

RESULTS

Influence of Flexion Only

Microscopic examination of the 12 reference segments flexed 10° without further compression showed no evidence of disc wall damage.

Influence of Flexion and Low Compression Rate

Endplate fracture occurred in all of the segments tested at the low loading rate whether neutral or flexed (Table 2). Endplate failure was associated with a sharp, audible cracking sound, sudden loss of disc height, and a simultaneous large drop in the load displacement curve (Figure 3, curve A). Macroscopic and microscopic evidence for this mode of fracture is shown in Figure 4A, B with intravertebral disc prolapse of nuclear material consistent with previous descriptions of disc decompression.[25,26] Importantly, our study showed no evidence of disc wall damage in these segments.

Influence of Flexion and High Compression Rate

All segments tested at the high rate in the neutral posture experienced endplate fracture as described in the earlier text. By contrast, approximately 50% of those segments flexed and compressed at the high rate experienced wall damage/failure, the remainder endplate fracture. Wall damage was associated with an irregular tearing sound that correlated with an erratic fall in the load displacement curve (curve B in Figure 3). If the loading was continued, an eventual precipitous drop in load-signaled facet joint fracture and thus gross failure of the motion segment. In the majority of cases in which wall damage occurred, the loading was terminated in the early phase of failure so as to capture the evolution of structural disruption (curve C in Figure 3).

There was no statistically significant difference ($P > 0.05$) between the average load required to induce endplate fracture in the neutral posture (11.5 kN) and that for endplate fracture in the flexed segments (10.1 kN). However, the average load required to induce herniation in flexion (8.9 kN) was significantly lower than that required for endplate fracture (10.9 kN), whether neutral or flexed ($P < 0.05$). There was no significant difference in average failure load between the 3 spinal levels ($P > 0.05$).

Microscopic Analysis of Disc Wall Failure

In the 13 samples that experienced disc wall failure (Table 3), 9 were located in the posterior annulus and 4 in the posterolateral annulus. By halting the compression at different displacement points after initial failure, varying degrees of microstructural disruption were obtained.

Figure 5 demonstrates limited annular failure in a specimen where loading was interrupted immediately after

Copyright © 2014 Lippincott Williams & Wilkins. Unauthorized reproduction of this article is prohibited.

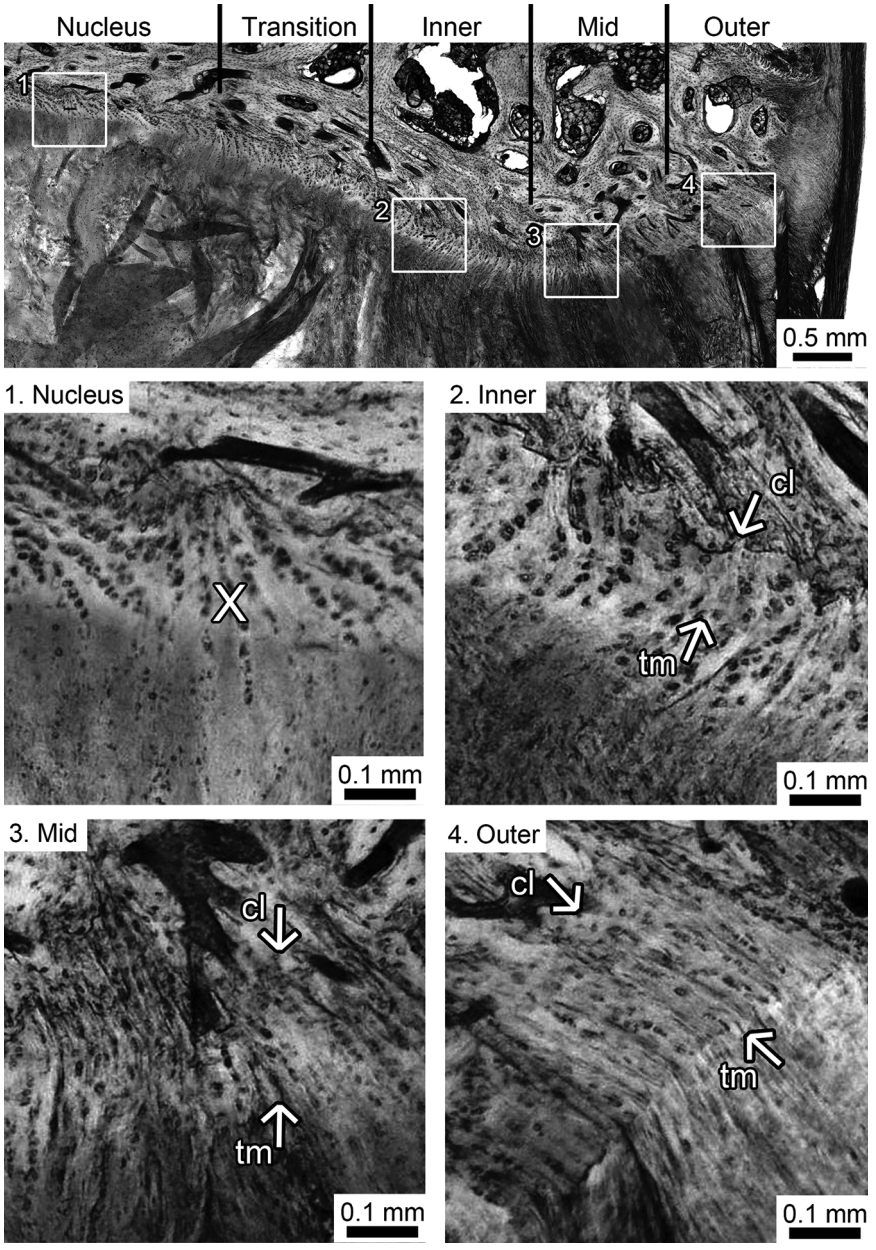

Figure 2. *Upper image*: central sagittal section of the superior disc/endplate showing the relevant regions in the posterior aspect. *Lower images*: enlarged views of the 4 boxed regions in the nucleus, inner, middle, and outer annulus. Box 1 shows the insertion nodes (X) integrating the nucleus and cartilaginous endplate[27]; boxes 2 to 4 show an increasing thickness of the calcified cartilaginous endplate seen by comparing the separation distance between the 2 arrows indicating the tm and cl. Tm indicates tidemark; cl, cement line.

reduction in the gradient of the load displacement curve (*i.e.*, as in curve C in Figure 3). It represents the earliest phase of annular disruption. The relatively mild damage is largely concentrated within the lamellae of the mid-then-outer annulus, with minor tearing of the annular bundles in Figure 5 A-D (between arrows) and limited nuclear migration at the asterisked sites in Figure 5A, B. There is no endplate involvement.

TABLE 1. Numbers of Motion Segments Tested at Each Posture and Compression Rate

	Neutral	Flexed (10°)
Reference segments (subjected to flexion only)	N.A.	12 segments from 4 spines
Segments tested to failure at low compression rate	8 segments from 3 spines	9 segments (3 spines)
Segments tested to failure at high compression rate	19 segments (7 spines)	24 segments (8 spines)

N.A. indicates not applicable.

Figure 6 shows a subligamentous herniation from a segment in which loading was terminated prior to facet joint failure and thus representing a more severe degree of annular disruption. The video recording showed the posterior ligament initially rippling then bulging but not breached by herniated material. Imaged both in the sagittal midline of the sample (Figure 6A) and in an offset lateral sagittal slice (Figure 6B), we see both midannulur-endplate tearing (see enlargement in Figure 6C) and midspan lamellae rupture in the mid and outer annulus (see arrows in Figure 6B). Midannular-endplate failure has proceeded *via* an interdigitated separation along both the tidemark and the cement line (Figure 6C), and there is extensive tearing of the cartilaginous endplate along its tidemark in the inner annulus-nucleus region (see asterisked sites in Figure 6A, B).

Copyright © 2014 Lippincott Williams & Wilkins. Unauthorized reproduction of this article is prohibited.

TABLE 2. Summary of Damage Type and Failure Loads in Relation to Posture and Compression Rate

Posture and compression rate	Endplate Failure		Disc Herniation	
	Number	Load at failure, Mean (Range)	Number	Load at Failure, Mean (Range)
Neutral + low rate	8	7.94 kN (5.9–9.6)	0	N.A.
Flexed + low rate	9	9.4 kN (7.5–11.6)	0	N.A.
Neutral + high rate	19	11.5 kN (8.7–15.6)	0	N.A.
Flexed + high rate	11	10.1 kN (6.4–15)	13	8.9 kN (4.9–14.2)

N.A. indicates not applicable.

Figure 7A is a centrally located sagittal section through a full transligamentous herniation in a motion segment that had been extensively compressed to facet fracture. The mid and outer annular lamellae have ruptured in midspan (between the arrows) but without obvious subjacent endplate failure. However, there is extensive tearing of the cartilaginous endplate at the tidemark in the inner annulus-nucleus transition zone (see LH (left hand) side asterisks). The extrusion of nucleus and endplate material has resulted in the destruction of the posterior ligament. The RH (right hand) asterisked site demarcates a band of mineralized tissue and associated inner annulus-nucleus originating from the LH side asterisked site. On becoming partially detached, this material has inverted during extrusion while remaining tenuously attached to residual inner annulus/nucleus.

Figure 7B, C show equivalent but laterally offset sagittal views of this transligamentous herniation, confirming its focal nature. Figure 7B shows nucleus protruding radially as far as the outermost lamellae (see horizontal arrow). There is also extensive tearing of the cartilaginous endplate in the inner region (shorter white arrows). With the greater offset in Figure 7C, there is a lesser degree of nuclear protrusion and inner endplate tearing with the displaced material appearing to weave an irregular path around the midannular bundles (see region between arrows).

DISCUSSION

Despite the frequency of disc herniations, annular tears, and endplate injuries, their pathogenesis remains unclear. Biomechanically, a fully hydrated disc loaded at a high rate would

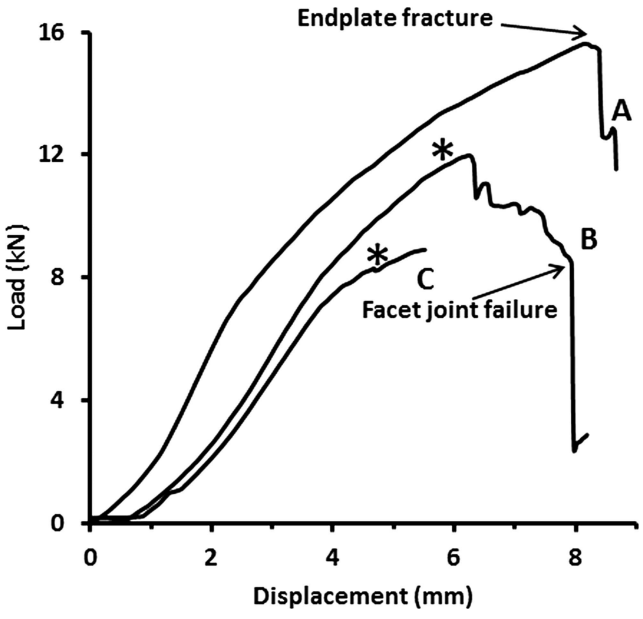

Figure 3. Typical load *versus* displacement curves from 3 motion segments, one failing in unflexed posture (curve A) *via* endplate fracture, and the other 2 by disc wall failure. Curve B was a full transligamentous herniation, and in curve C loading was halted immediately following first evidence of failure. Asterisks indicate the approximate commencement of audible fiber rupture.

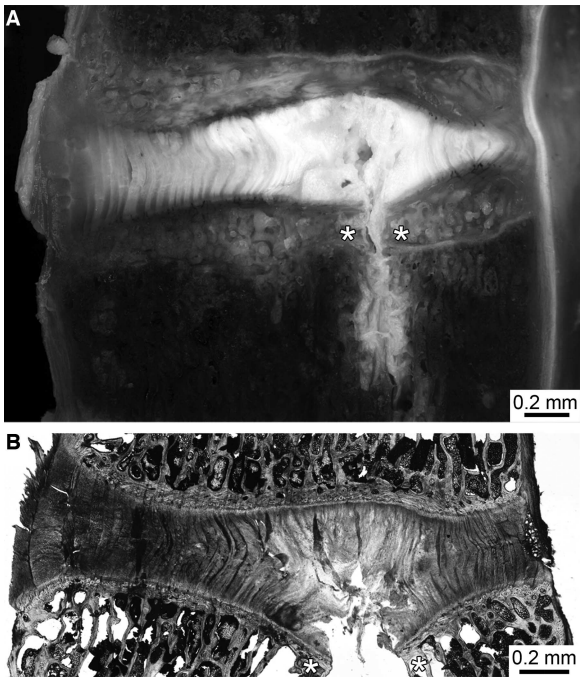

Figure 4. Macrolevel (**A**) and microstructural (**B**) views of typical endplate fractures. The inferior vertebral endplate can be seen to have fractured subjacent to the midnucleus (**) allowing the nucleus to be extruded into the vertebral body. In this mode of failure there is no obvious damage to the walls of the annulus.

Copyright © 2014 Lippincott Williams & Wilkins. Unauthorized reproduction of this article is prohibited.

TABLE 3. Failure Data From Motion Segments Compressed in Flexion (10°) at the Higher Rate

Motion Segment	Failure Load (kN)	Endplate Fusion	Herniation Phase Captured	Failure Mode	Transverse Location of Wall Failure	Wall Damage Morphology
Spine 1, L1–L2	11.78	Fused	Late	Disc wall	Posterior	MS + IT + SL
Spine 1, L3–L4	10.89	Fused	Late	Disc wall	Posterior	MS + IT + SL
Spine 1, L5–L6	6.1	Fused	Late	Disc wall	Posterior	MS + TL
Spine 2, L1–L2	12.54	Fused	N/A	Endplate	N/A	N/A
Spine 2, L3–L4	15	Fused	N/A	Endplate	N/A	N/A
Spine 2, L5–L6	14.2	Fused	Late	Disc wall	Posterior	MS + SL
Spine 3, L1–L2	4.86	Fused	Mid	Disc wall	Posterior	AE + NF
Spine 3, L3–L4	6.66	Fused	Mid	Disc wall	Posterior	AE + IT + SL
Spine 3, L5–L6	6.73	Fused	Mid	Disc wall	Posterolateral	WT + SL
Spine 4, L1–L2	10.46	Unfused	N/A	Endplate	N/A	N/A
Spine 4, L3–L4	8.69	Unfused	N/A	Endplate	N/A	N/A
Spine 4, L5–L6	9.54	Unfused	N/A	Endplate	N/A	N/A
Spine 5, L1–L2	6.41	Unfused	N/A	Endplate	N/A	N/A
Spine 5, L3–L4	9.71	Unfused	N/A	Endplate	N/A	N/A
Spine 5, L5–L6	7.85	Unfused	N/A	Endplate	N/A	N/A
Spine 6, L1–L2	7.6	Unfused	Early	Disc wall	Posterior	MS + IT + SL
Spine 6, L3–L4	7.18	Unfused	Early	Disc wall	Posterolateral	AE + IT + SL
Spine 6, L5–L6	11.64	Unfused	Early	Disc wall	Posterolateral	AE + SL
Spine 7, L1–L2	8.25	Unfused	Early	Disc wall	Posterolateral	WT + NF
Spine 7, L3–L4	11.69	Unfused	N/A	Endplate	N/A	N/A
Spine 7, L5–L6	10.65	Unfused	Early	Disc wall	Posterior	AE + SL
Spine 8, L1–L2	9.12	Fused	N/A	Endplate	N/A	N/A
Spine 8, L3–L4	9.7	Fused	N/A	Endplate	N/A	N/A
Spine 8, L5–L6	8.9	Fused	Early	Disc wall	Posterior	WT
Mean	Endplate: 10.1 annulus: 8.9					

Failures are classified by the following criteria: endplate fused/unfused, herniation phase captured (early/mid/late), disc wall failure/endplate fracture, transverse location, i.e., posterior/posterolateral, wall damage morphology.

WT indicates diffuse annular rupture/tearing; MS, midspan annular rupture; AE, annular-endplate rupture; IT, inner annulus/endplate tearing; NP, nuclear protrusion; SL, subligamentous nuclear extrusion; TL, transligamentous nuclear extrusion.

likely experience damage,[27] yet published images of clinical herniations are more generally associated with degenerative changes.[28–31]

The debate as to whether the disc is normal or degenerated at the time of herniation continues.[10,32–34] Annulus-endplate junction failure is increasingly accepted as a further mechanism of disc failure/injury and there is increasing *in vitro* and clinical support for this.[16,35] Improved imaging of the nucleus and annulus, along with *in vitro* disc pressurization leading to failure, provides insight into endplate/annular failure patterns.[14–17] However, to our knowledge trauma-related mechanisms of disc disruption at the microstructural level, and the evolution of herniation, have not been elucidated using direct compression of motion segments in realistic postures. The aim of this study was to address this issue.

It is clear from the 12 reference motion segments that 10° of flexion alone does not disrupt the disc, an observation that is consistent with the earlier findings of Veres *et al*.[15] This confirms that the degree of flexion used in this new study is physiologically realistic. Conversely, we show that an elevated rate of compression (comparable with that used to achieve herniation in hyperflexed discs[10]), combined with this level of flexion, are critical factors in promoting wall disruption and herniation because without both of these the motion segments invariably failed *via* endplate fracture (Table 2).

Copyright © 2014 Lippincott Williams & Wilkins. Unauthorized reproduction of this article is prohibited.

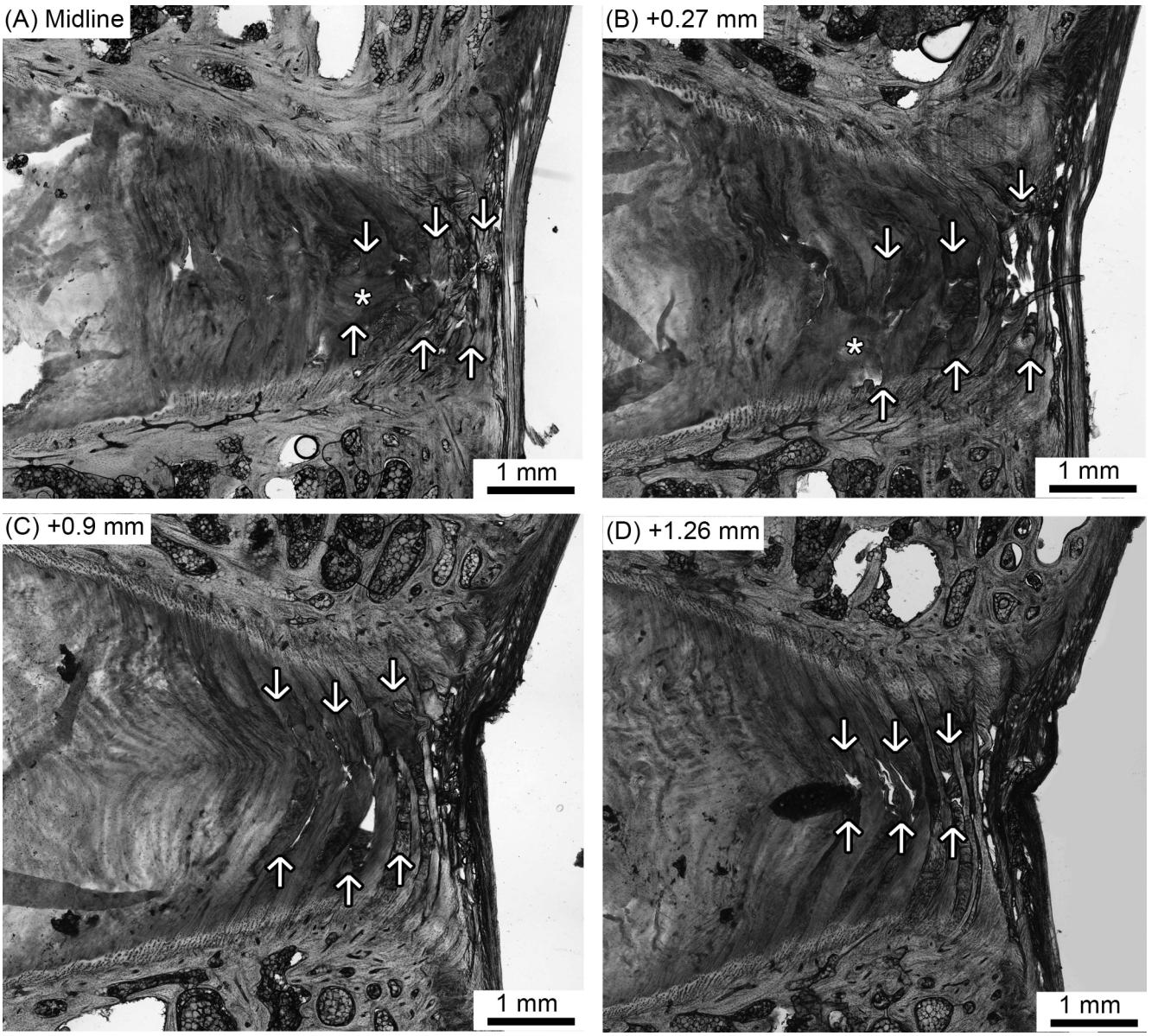

Figure 5. A series of sagittal sections with varying degrees of offset (amount of offset indicated in top LH corner of each image) through the posterior-mediolateral region of a disc that exhibited no outward signs of damage during loading. Arrows highlight main regions of annular failure (**A-D**). Asterisks indicate early nuclear displacement (**A** and **B** only).

Our data indicate that a significantly lower load was required to induce disc failure compared with that require for endplate fracture at the high rate of compression when combined with flexion. This clearly exposes the inherent variability in strength of the healthy disc. Further, only half of the discs tested in flexion (which was at the upper extreme of the physiological range) experienced wall damage when overloaded in compression. This supports the assertion in the published literature that some seemingly normal discs are more susceptible to herniation than others.[32,34,36]

Focusing now on our microstructural evidence, some common features of the process leading to disc failure can be identified. First, the mid-to-outer annulus experienced damage in all discs that underwent wall failure, thus indicating that it is this region that is damaged first and thus most vulnerable to combined compressive overloading and flexion. This damage can occur by midspan rupture of the lamellar bundles (Figures 6B or 7) and by separation at the tidemark or along the cement line (Figure 6C). The extent of this disruption could influence the pathway taken by the resulting herniation: many relatively small midannular tears would very likely produce diffuse herniations[11,17,37] shown at an incipient stage in Figure 5. Conversely, the larger tears observed in the midregions of the more severely damaged discs (Figures 6, 7) would provide a more direct path for extrusion.

Second, the inner annulus seems to be the next structure to experience damage, with tearing and disruption of the layers, which, in their semidetached state, are then forced outward

Copyright © 2014 Lippincott Williams & Wilkins. Unauthorized reproduction of this article is prohibited.

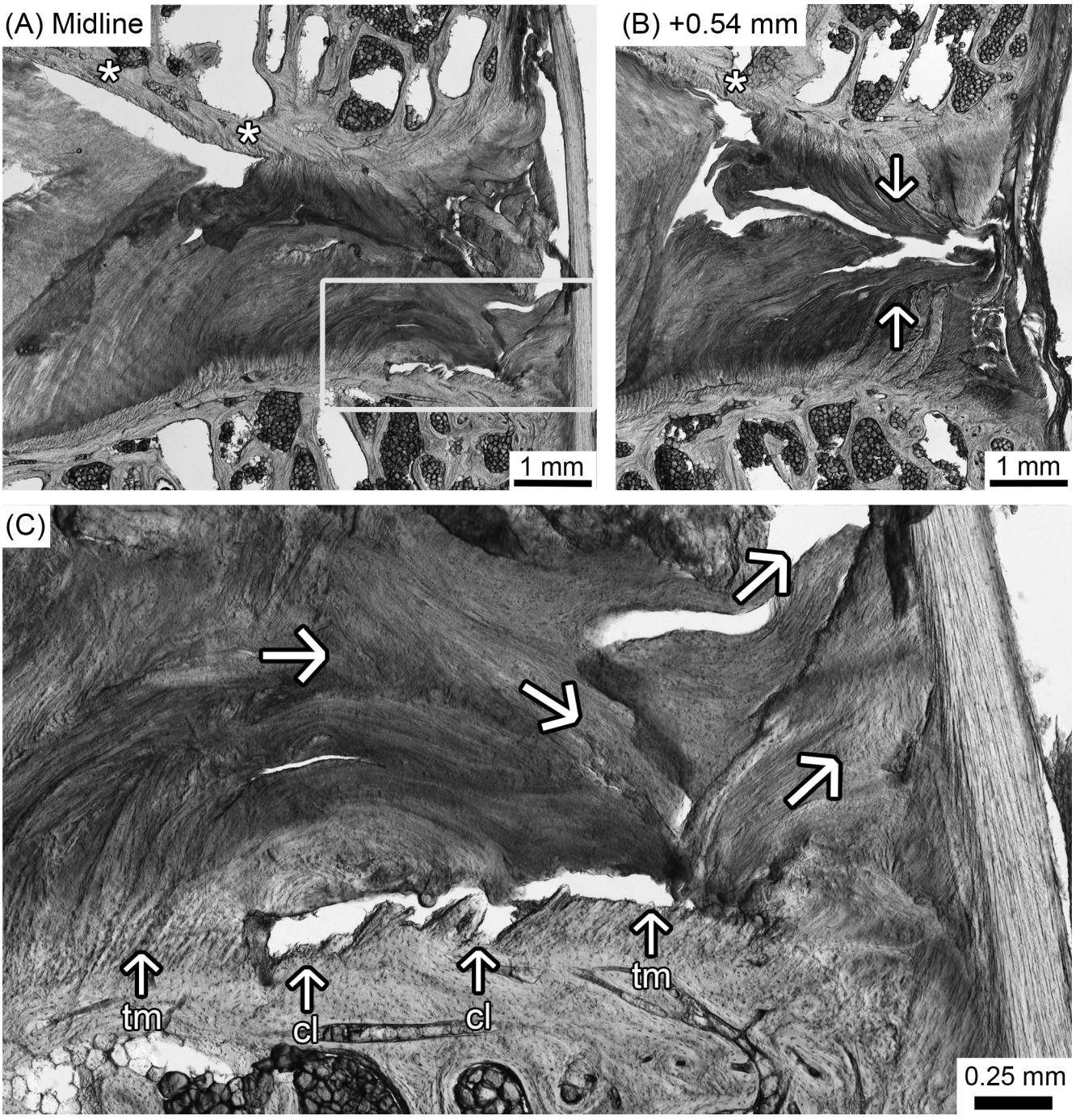

Figure 6. A series of sagittal sections through the posterior-mediolateral region of a disc that failed *via* a subligamentous herniation. The boxed region in the central sagittal view in (**A**) is shown at a higher magnification in (**C**). Note that damage is present in both the annulus-endplate junction (**A**) and in the midspan annulus (offset image **B**). tm indicates tidemark; cl, cement line.

through the already damaged mid-to-outer annulus by the pressure-displaced nuclear material. This process is accompanied by tearing of the annulus/cartilaginous endplate or nucleus/endplate junction at the tidemark as evidenced by the extruded material containing torn endplate fragments (Figures 6, 7). These images correlate with the frequent finding of cartilaginous endplate material within the mass of herniation tissue seen at surgery.[38,39]

Lastly, the images in Figure 7B and C capture the extent of protrusion adjacent to the focal sagittal plane of the full transligamentous extrusion in Figure 7A. The severely displaced nuclear material has broken through all but the outermost lamellae and posterior ligament and therefore provides a sequential glimpse at the microstructural level of the evolution of wall failure. It should be noted that although facet failure was common in the discs that experienced transligamentous

Copyright © 2014 Lippincott Williams & Wilkins. Unauthorized reproduction of this article is prohibited.

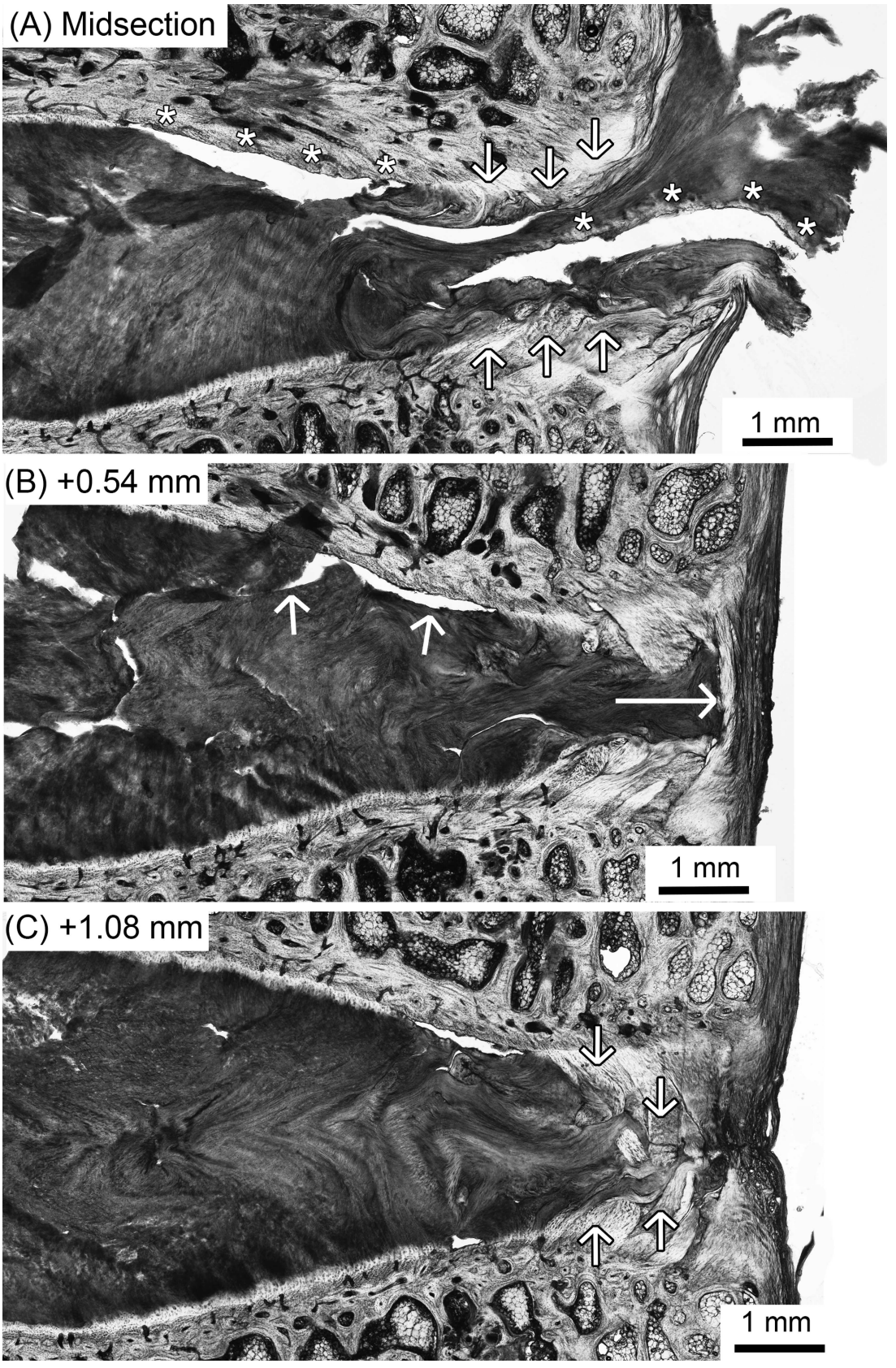

Figure 7. A series of central sagittal (**A**) and offset (**B**, **C**) sections through the posterior-mediolateral region of a disc that failed *via* a transligamentous herniation. The reduction in extent of nuclear protrusion with increasing lateral offset is clearly visible (offset indicated in top LH corner).

Copyright © 2014 Lippincott Williams & Wilkins. Unauthorized reproduction of this article is prohibited.

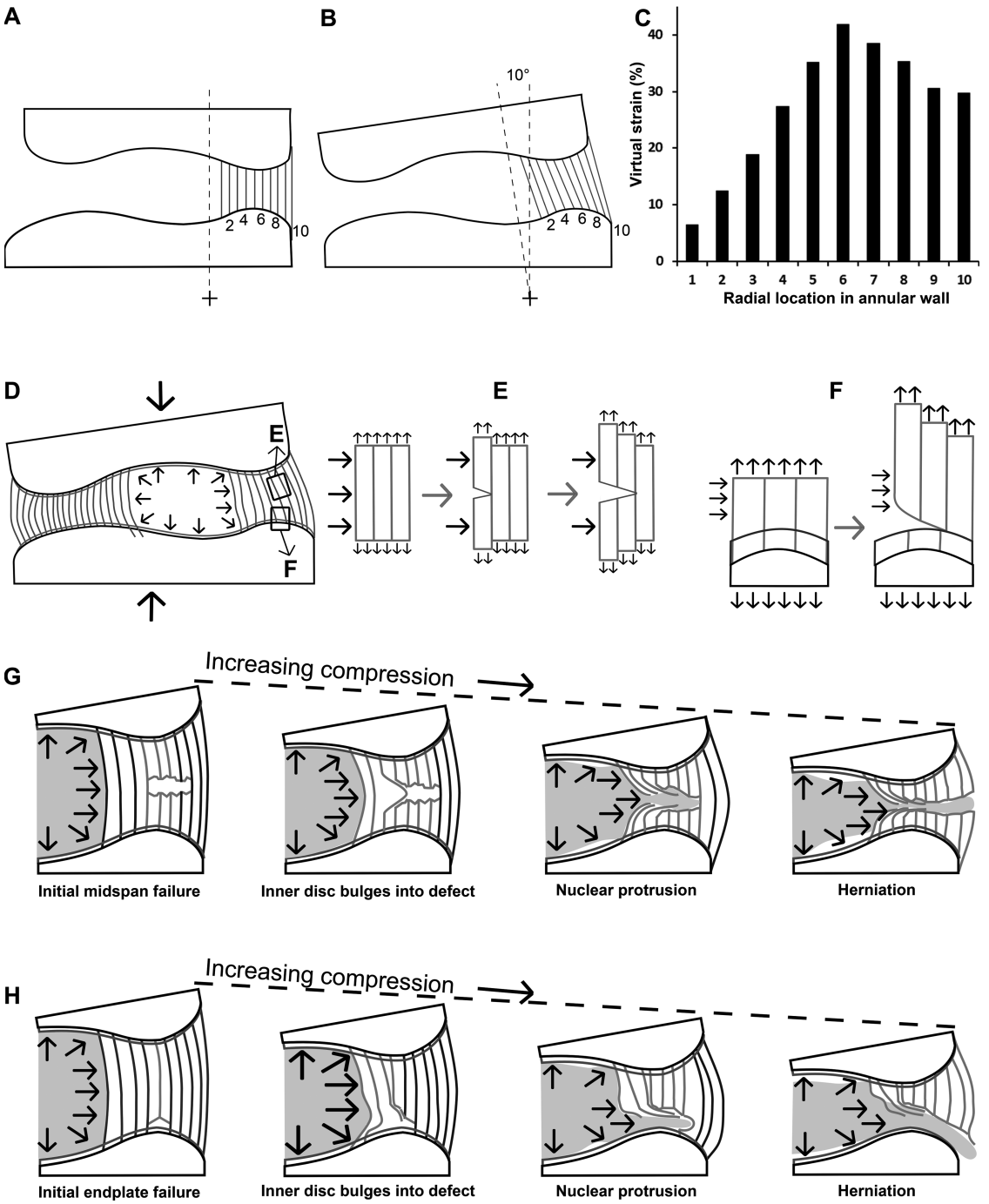

Figure 8. **A**, **B** illustrate the virtual displacement of points on the endplates due to 10° flexion (axis of rotation is marked +). The corresponding virtual strains in the posterior annular wall resulting from this flexion are shown in (**C**). The most highly stressed midregion (**D**) can fail *via* 2 mechanisms, either midspan rupture (**E**) or annular-endplate tearing (**F**). The disruptive stages leading to herniation, resulting from these 2 distinct failure modes, are shown in (**G**) and (**H**), respectively.

herniations (which is not the case *in vivo*) this is likely to be a consequence of the loss of disc height after extensive herniation, the latter occurring too rapidly to halt the test before the facets fracture.

We propose that the earlier described sequence of events leading to disc failure is linked to endplate geometry. An outline traced from an actual disc and its endplates is shown in Figure 8A. Because of the endplate ridge apex the midannular region will have the shortest endplate-to-endplate span. If we flex the motion segment about a center of rotation located in the inferior vertebral body[40,41] (Figure 8B) it is possible to calculate the virtual displacements of the corresponding points (1–10) on the opposing endplates due to this flexion. The virtual strains between the points can be calculated and

Copyright © 2014 Lippincott Williams & Wilkins. Unauthorized reproduction of this article is prohibited.

shown as a distribution across the width of the annular wall (Figure 8C). These high strains will, of course, be prevented by the intrinsic strain-limiting properties of the annulus. However the plotted strain distribution does provide a clear indication of those lamellae that would be loaded first in flexion that is those in the mid-then-outer annulus.

One additional factor must be considered: as the oblique fiber angle increases from the outer to the inner layers, this will add further to the midannular strains relative to the outer fibers. Combining these factors we argue that in flexion the midannular fibers followed by the outer layer fibers will be most heavily stressed and therefore most vulnerable when exposed to the bulging of the inner disc under compression (Figure 8D).

Natural structural variations arising from local differences in fiber packing density, incomplete lamellae,[42] or even partial tears in the lamellae due to previous damage, could act as further sites of stress concentration thereby initiating rupture in the midannulus. A progressive transfer of load into adjacent intact annular elements, which then fail, would advance the damage as fewer fibers now carry more of the applied load. This mechanism is illustrated in Figure 8E.

Failure in the midannulus also involved the annular-endplate junction (Figure 6C). This region is a rigid anchorage for the flexible annular fibers integrating the compliant disc and vertebral body. Stress concentrations are inevitable in such systems with large step changes in material stiffness. The significant amount of delamination observed along both the tidemark and the cement line is certainly consistent with the interpretation given in the earlier text and is illustrated schematically in Figure 8F. A similar mechanism would explain why in Figure 7A there is endplate material attached to the herniated mass derived from the nucleus-inner annulus, a region known to be structurally integrated with its surroundings.[43–45]

Earlier studies[46–51] have shown that the interior of the disc, that is, the inner annulus and nucleus, behaves hydrostatically as a "functional nucleus." Combining this concept with our microstructural evidence, the series of schematics in Figure 8G and H depict the probable sequence of events leading to herniation in the flexed disc: after damage to the highly stressed mid-to-outer annulus, the inner annulus, and nucleus bulge into the defect. Further loading acts to increase these effects, probably accompanied by tearing of the inner annulus/cartilaginous endplate junction with associated nuclear protrusion. Still more loading will cause further displacement of the inner disc material into the outer annular regions that are in turn disrupted, leading eventually to a transligamentous herniation.

Conversely, if loading is halted at the incipient stage of damage (Figure 5) the minor tears could provide a weak point for future herniation. They could also trigger the degenerative cascade in the disc and lead to the rim lesions identified by Osti *et al*.[30,31] Further, given the subtle nature of this incipient damage and the limited innervation of the outer disc,[52] it is plausible that this early phase could be asymptomatic.

CONCLUSION

This study has shown that flexed ovine motion segments compressed at elevated loading rates can experience structural damage that mimics disc herniation in life. Disc wall failure seems to commence in the mid-then-outer annulus. We propose that the convex geometry of the posterior endplate ridge results in higher fiber strains in the mid-then-outer annulus with their eventual failure leading to full herniation. Given the similarity in geometry between ovine and human endplates[20,22,53,54] it is likely that comparable mechanisms of damage initiation and herniation operate in humans although further investigations will be required to confirm this. The influence of even higher compression rates, added minor components of torsion,[14,15,55] as well as lower levels of cyclic compression, remain yet to be explored.

➢ Key Points

- ❑ A combination of flexion and an elevated rate of compression is required to produce herniation in healthy ovine discs.
- ❑ The mid-then-outer regions of the annulus were damaged first in motion segments that experienced disc wall failure.
- ❑ Damage to the inner annulus/endplate junction and the outer peripheral annular lamellae occurred in the later stages of disc failure.
- ❑ It is proposed that the initiation of disc wall failure is due to the geometry of the endplate creating high fiber strains in the mid-then-outer posterior annular lamellae when the disc is flexed, thus rendering them most vulnerable to rupture.

References

1. Porchet F, Wietlisbach V, Burnand B, et al. Relationship between severity of lumbar disc disease and disability scores in sciatica patients. *Neurosurgery* 2002;50:1253–60.
2. Weber H. Lumbar disc herniation. A controlled, prospective study with ten years of observation. *Spine* 1983;8:131–40.
3. Arts MP, Peul WC, Koes BW, et al. Management of sciatica due to lumbar disc herniation in the Netherlands: a survey among spine surgeons. *J Neurosurg Spine* 2008;9:32–9.
4. Yoganandan N, Maiman DJ, Pintar F, et al. Microtrauma in the lumbar spine: a cause of low back pain. *Neurosurgery* 1988;23:162–8.
5. Rolander SD, Blair WE. Deformation and fracture of the lumbar vertebral endplate. *Orthop Clin N Am* 1975;6:75–81.
6. Roaf R. A study of the mechanics of spinal injuries. *J Bone Joint Surg Br* 1960;42-B:810–23.
7. Lin HS, Liu YK, Adams KH. Mechanical response of the lumbar intervertebral joint under physiological (complex) loading. *J Bone Jt Surg Ser A* 1978;60 A:41–55.
8. Brown T, Hansen RJ, Yorra AJ. Some mechanical tests on the lumbosacral spine with particular reference to the intervertebral discs; a preliminary report. *J Bone Jt Surg Am* 1957;39 A:1135–64.
9. Lundin O, Ekström L, Hellström M, et al. Injuries in the adolescent porcine spine exposed to mechanical compression. *Spine* 1998;23:2574–9.
10. Adams MA, Hutton WC. Prolapsed intervertebral disc: a hyperflexion injury. *Spine* 1982;7:184–91.
11. Adams MA, Hutton WC. Gradual disc prolapse. *Spine* 1985;10:524–31.

Copyright © 2014 Lippincott Williams & Wilkins. Unauthorized reproduction of this article is prohibited.

12. Adams MA, Hutton WC. The mechanics of prolapsed intervertebral disc. *Int Orthop* 1982;6:249–53.
13. McNally DS, Adams MA, Goodship AE. Can intervertebral disc prolapse be predicted by disc mechanics? *Spine* 1993;18:1525–30.
14. Veres SP, Robertson PA, Broom ND. The influence of torsion on disc herniation when combined with flexion. *Eur Spine J* 2010;19:1468–78.
15. Veres SP, Robertson PA, Broom ND. The morphology of acute disc herniation: a clinically relevant model defining the role of flexion. *Spine* 2009;34:2288–96.
16. Veres SP, Robertson PA, Broom ND. ISSLS prize winner: How loading rate influences disc failure mechanics: a microstructural assessment of internal disruption. *Spine* 2010;35:1897–908.
17. Veres SP, Robertson PA, Broom ND. ISSLS prize winner: microstructure and mechanical disruption of the lumbar disc annulus: part II: how the annulus fails under hydrostatic pressure. *Spine* 2008;33:2711–20.
18. Thompson JP, Pearce RH, Schechter MT, et al. Preliminary evaluation of a scheme for grading the gross morphology of the human intervertebral disc. *Spine* 1990;15:411–5.
19. Adams MA, Hutton WC. The effect of posture on the role of the apophysial joints in resisting intervertebral compressive forces. *J Bone Jt Surg Ser B* 1980;62:358–62.
20. Wilke HJ, Kettler A, Wenger KH, et al. Anatomy of the sheep spine and its comparison to the human spine. *Anatomical Record* 1997;247:542–55.
21. Reid JE, Meakin JR, Robins SP, et al. Sheep lumbar intervertebral discs as models for human discs. *Clin Biomech* 2002;17:312–4.
22. Wilke HJ, Kettler A, Claes LE. Are sheep spines a valid biomechanical model for human spines? *Spine* 1997;22:2365–74.
23. Smit TH. The use of a quadruped as an *in vivo* model for the study of the spine—Biomechanical considerations. *Eur Spine J* 2002;11:137–44.
24. Race A, Broom ND, Robertson P. Effect of loading rate and hydration on the mechanical properties of the disc. *Spine* 2000;25:662–9.
25. Lundin O, Ekström L, Hellström M, et al. Exposure of the porcine spine to mechanical compression: Differences in injury pattern between adolescents and adults. *Eur Spine J* 2000;9:466–71.
26. Adams MA, Hutton WC. The effect of posture on the lumbar spine. *J Bone Jt Surg Ser B* 1985;67:625–9.
27. Adams MA, Dolan P. Recent advances in lumbar spinal mechanics and their clinical significance. *Clin Biomech* 1995;10:3–19.
28. Yasuma T, Koh S, Okamura T, et al. Histological changes in aging lumbar intervertebral discs. Their role in protrusions and prolapses. *J Bone Jt Surg Ser A* 1990;72:220–9.
29. Yasuma T, Makino E, Saito S, et al. Histological development of intervertebral disc herniation. *J Bone Jt Surg Ser A* 1986;68:1066–72.
30. Osti OL, Vernon-Roberts B, Fraser RD. 1990 Volvo award in experimental studies: annulus tears and intervertebral disc degeneration: an experimental study using an animal model. *Spine* 1990;15:762–7.
31. Osti OL, Vernon-Roberts B, Moore R, et al. Annular tears and disc degeneration in the lumbar spine: a post- mortem study of 135 discs. *J Bone Jt Surg Ser B* 1992;74:678–82.
32. Lama P, Le Maitre CL, Dolan P, et al. Do intervertebral discs degenerate before they herniate, or after? *Bone Jt J* 2013;95 B:1127–33.
33. Videman T, Nurminen M, Troup JDG. 1990 Volvo award in clinical sciences: lumbar spinal pathology in cadaveric material in relation to history of back pain, occupation, and physical loading. *Spine* 1990;15:728–40.
34. Battié MC, Videman T, Levälahti E, et al. Genetic and environmental effects on disc degeneration by phenotype and spinal level: a multivariate twin study. *Spine* 2008;33:2801–8.
35. Rajasekaran S, Bajaj N, Tubaki V, et al. ISSLS prize winner: the anatomy of failure in lumbar disc herniation: an *in vivo*, multimodal, prospective study of 181 subjects. *Spine* 2013.
36. Adams MA, Roughley PJ. What is intervertebral disc degeneration, and what causes it? *Spine* 2006;31:2151–61.
37. Tampier C, Drake JDM, Callaghan JP, et al. Progressive disc herniation: an investigation of the mechanism using radiologic, histochemical, and microscopic dissection techniques on a porcine model. *Spine* 2007;32:2869–74.
38. Harada Y, Nakahara S. A pathologic study of lumbar disc herniation in the elderly. *Spine* 1989;14:1020–4.
39. Moore RJ, Vernon-Roberts B, Fraser RD, et al. The origin and fate of herniated lumbar intervertebral disc tissue. *Spine* 1996;21:2149–55.
40. Pearcy MJ, Bogduk N. Instantaneous axes of rotation of the lumbar intervertebral joints. *Spine* 1988;13:1033–41.
41. Yoshioka T, Tsuji H, Hirano N, et al. Motion characteristic of the normal lumbar spine in young adults: instantaneous axis of rotation and vertebral center motion analyses. *J Spinal Disord* 1990;3:103–13.
42. Marchand F, Ahmed AM. Investigation of the laminate structure of lumbar disc annulus fibrosus. *Spine* 1990;15:402–10.
43. Wade K, Robertson P, Broom N. A fresh look at the nucleus-endplate region: new evidence for significant structural integration. *Eur Spine J* 2011;20:1225–32.
44. Wade KR, Robertson PA, Broom ND. On the extent and nature of nucleus-annulus integration. *Spine* 2012;37:1826–33.
45. Wade KR, Robertson PA, Broom ND. On how nucleus-endplate integration is achieved at the fibrillar level in the ovine lumbar disc. *J Anatomy* 2012;221:39–46.
46. Nachemson A. Towards a better understanding of low back pain: a review of the mechanics of the lumbar disc. *Rheumatol Rehabil* 1975;14:129–43.
47. Nachemson A. Lumbar intradiscal pressure. Experimental studies on post-mortem material. *Acta Orthop Scand Suppl* 1960;43:1–104.
48. Adams MA, McNally DS, Wagstaff J, et al. Abnormal stress concentrations in lumbar intervertebral discs following damage to the vertebral bodies: a cause of disc failure? *Eur Spine J* 1993;1:214–21.
49. Adams MA, McNally DS, Dolan P. "Stress" distributions inside intervertebral discs. The effects of age and degeneration. *J Bone Jt Surg Ser B* 1996;78:965–72.
50. McNally DS, Adams MA. Internal intervertebral disc mechanics as revealed by stress profilometry. *Spine* 1992;17:66–73.
51. McMillan DW, Garbutt G, Adams MA. Effect of sustained loading on the water content of intervertebral discs: implications for disc metabolism. *Ann Rheum Dis* 1996;55:880–7.
52. Palmgren T, Grönblad M, Virri J, et al. An immunohistochemical study of nerve structures in the annulus fibrosus of human normal lumbar intervertebral discs. *Spine* 1999;24:2075–9.
53. Twomey LT, Taylor JR. Age changes in lumbar vertebrae and intervertebral discs. *Clin Orthop Relat Res* 1987:97–104.
54. Francois RJ, Dhem A. Microradiographic study of the normal human vertebral body. *Acta Anat (Basel)* 1974:251–65.
55. Adams MA, Hutton WC. The relevance of torsion to the mechanical derangement of the lumbar spine. *Spine* 1981;6:241–7.

Copyright © 2014 Lippincott Williams & Wilkins. Unauthorized reproduction of this article is prohibited.